


Article

Study on the Mechanical Characteristics and Ground Surface Settlement Influence of the Rise–Span Ratio of the Pile–Beam–Arch Method

Jianbing Lv ^{*}, Jianjun Lu and Hao Wu

School of Civil and Transportation Engineering, Guangdong University of Technology, Guangzhou 510000, China; 2112109153@mail2.gdut.edu.cn (J.L.); 2112109006@mail2.gdut.edu.cn (H.W.)

* Correspondence: ljb@gdut.edu.cn; Tel.: +86-139-2628-8216

Abstract: The pile–beam–arch method (PBA) method is increasingly being used in the construction of metro stations with complex traffic conditions. The rise–span ratio of the arch not only affects the height of the station, but also affects the rationality of the design of subway stations and the safety of construction. The mechanical response of steel pipe piles with different rise–span ratios and the effect of controlled surface settlement have been investigated in the interactions involved in pile–soil system. In this paper, the finite element model of each rise–span ratio was established, and the rationality of the model was demonstrated by comparing the numerical simulation calculation with the field surface settlement monitoring data. The mechanical characteristics and influence analysis of the surface deformation during the excavation of the cave pile method were investigated. The results show that the maximum axial force of the central pile first decreases and then increases with the increase in the rise–span ratio. The maximum bending moment of the arch decreases as the rise–span ratio increases, and the maximum axial force of the arch is negatively correlated with the rise–span ratio. The maximum axial force of the central pile is located at the bottom plate. Due to the symmetry of the structure, the bending moment of the centre pile is small, but the maximum bending moment of the whole station is located at the side wall of the bottom plate. As the rise–span ratio increases, the surface settlement first decreases and then increases. The construction of the pilot tunnel and the upper arch is the most important factor leading to the surface settlement, so it is necessary to strengthen the soil layer.

Keywords: subway station; pile–beam–arch method; rise–span ratio; finite element



Citation: Lv, J.; Lu, J.; Wu, H. Study on the Mechanical Characteristics and Ground Surface Settlement Influence of the Rise–Span Ratio of the Pile–Beam–Arch Method. *Appl. Sci.* **2023**, *13*, 5678. <https://doi.org/10.3390/app13095678>

Academic Editor: Arcady Dyskin

Received: 9 April 2023

Revised: 27 April 2023

Accepted: 28 April 2023

Published: 5 May 2023



Copyright: © 2023 by the authors. Licensee MDPI, Basel, Switzerland. This article is an open access article distributed under the terms and conditions of the Creative Commons Attribution (CC BY) license (<https://creativecommons.org/licenses/by/4.0/>).

1. Introduction

Throughout the history of subway construction, the open excavation method and the cover excavation method have been the most widely used methods for subway stations construction [1], especially for shallow underground tunnels, which have advantages in terms of cost, time, and safety. However, with the continuous development of engineering technology and the economic level, the pile–beam–arch (PBA) method has been widely used for the construction of subway stations [2–4] because of its good surface settlement control, convenient excavation mode [5], no need for large area excavation and filling, and no impact on the normal operation of road traffic. PBA is a technique based on the traditional concealed undercutting method, which integrates the characteristics of cover excavation method and forms a perfect frame bearing system of arch–beam–column before most of the soil has been excavated. The essence of the PBA method is to attempt to quickly form the overall framework, consisting of side piles (or side columns), steel pipe piles supporting the arch section, and then, under the protection of the arch structure, to excavate the sections [6,7]. The pile–beam–arch method of construction has lower ground disturbance and higher structural safety [8], which is particularly suitable for the construction of metro stations with heavy ground traffic, concentrated underground

pipelines and high ground settlement requirements [9,10]. The overturning resistance of the side piles, the compression and bending resistance of the steel pipe pile and the stability of the ground at the top of the arch are the keys to structural safety.

Although the pile–beam–arch method construction technology is widely used all over the world. The excavation of underground structures inevitably disturbs the initial stress field, redistributes the stress of the surrounding rock and leads to layer settlement or uplift. A number of problems need to be solved, such as the complex structural mechanics system conversion [8,11,12] of the pile–beam–arch method and tunnel instability in soft surrounding rocks and ground settlement [13,14]. Research methods on the mechanical properties and ground settlement of pile–beam–arch method subway stations mainly include model tests [10,15,16], numerical analysis [17–19], and field tests [20]. The pile–beam–arch method is used for large underground space projects. The advantage of this method is that it can minimize the ground loss caused by excavation and mitigate the damage to nearby buildings, and the pile–beam–arch method needs to be constructed inside the cavity, making the load-bearing structure inside the subway station particularly important. Therefore, the control of surface settlement is an important control factor for the construction of the pile–beam–arch method, for example, in the existing studies, the surface settlement of the excavation of the pilot tunnels and the construction of the arch structure in the construction of pile–beam–arch method accounts for about two-thirds of the total settlement [21,22], and even the value of this settlement reaches 90% [20]. There are, of course, many factors that affect the surface settlement, among which the maximum surface settlement is linearly related to the pile spacing. As the pile spacing increases, the maximum settlement increases; the maximum settlement decreases as the pile cross-section increases, and the economic cost should be reasonably controlled while the ground settlement is reasonably controlled [23]. In the case of unfavourable surrounding rock conditions, surface settlement can be effectively controlled by reducing the spacing of the side piles. When constructing the pile method of the double-connected arch cave with three pilot tunnels, the middle pilot tunnel can be constructed first, which can reduce the amount of surface settlement [24]. At present, the two most widely used methods for theoretical analysis of ground settlement calculations are the following: Peck's empirical equation method [25] and random media the theory method [26]. Based on the Peck curve, Lu [27], studied the law of ground settlement in the excavation of the two-lane subway tunnel and proposed a formula for calculating the lateral surface settlement. The key stage in the construction technology of the pile–beam–arch method is the construction of the pilot tunnel, so it has similarities with the excavation of the two-lane tunnel.

With the development of computers, finite elements can quickly solve approximate solutions to complex differential equations using the powerful computing power of computers to derive numerical values, making it a reliable tool for engineering design and analysis [28]. Finite elements can be used to predict geotechnical stability problems such as deep excavations, tunnels, vibrations, geological restoration, and other complex problems in civil engineering [29–31]. Minh [32] used the smooth finite element method to solve the stability problem of two circular tunnels at different depths in cohesive soils. Liang [33] solved the deformation problem of a very common discontinuity in rock engineering by the multi-body finite element method. Vazhbakht [34] optimised the finite element mesh to simplify the method of calculating stresses in the soil. The above studies show that the finite element method was applicable to the field of civil engineering and helps to solve difficult problems in geotechnical engineering and structural fields. Among them, because in the pile–beam–arch method, the ultimate load was transmitted through the arch structure and the longitudinal beam to the pile foundation, and finally the load was compensated by the pile side frictional resistance and the pile end resistance to ensure the stability of the structure. The pile and soil have obvious tangential slip and normal separation (or compression) tendency, so the pile–soil–structure interaction cannot be ignored [35,36]. In the actual finite element modelling analysis, the contact interface element can usually be set to simulate the pile–soil interaction.

In this paper, a three-dimensional finite element model of the pile–soil interaction interface was established to analyse the influence of different rise–span ratios on surface settlement to achieve the goal of settlement control. The mechanical characteristics of steel pipe piles and side piles are analysed by changing the arch rise–span ratio, and a reasonable rise–span ratio is proposed to reasonably optimize the building height of the station and improve the construction space of the station.

2. Practical Engineering Conditions

2.1. Pile–Beam–Arch Method Process

The metro station is located on a busy main road on Dong feng East Road in Guangzhou. In order not to disrupt the normal traffic and not to disturb the underground pipelines, the construction unit decided to use the pile–beam–arch method for the construction of the subway station. The design is a triple-arch structure, where the station is first constructed with three vertical shafts and excavated to each level. Then the cross-excavation was carried out along the cross-section of the metro station and the excavation in the construction cross-excavation was carried out up to the longitudinal section. The excavation of the three pilot tunnels was carried out first, followed by the construction of the centre pile, side pile and longitudinal beam, and then the construction of the upper arch. The construction of this arch structure is a key step in the formation of a stable underground frame structure using the pile–beam–arch method. The overall construction sequence is shown in Figure 1.

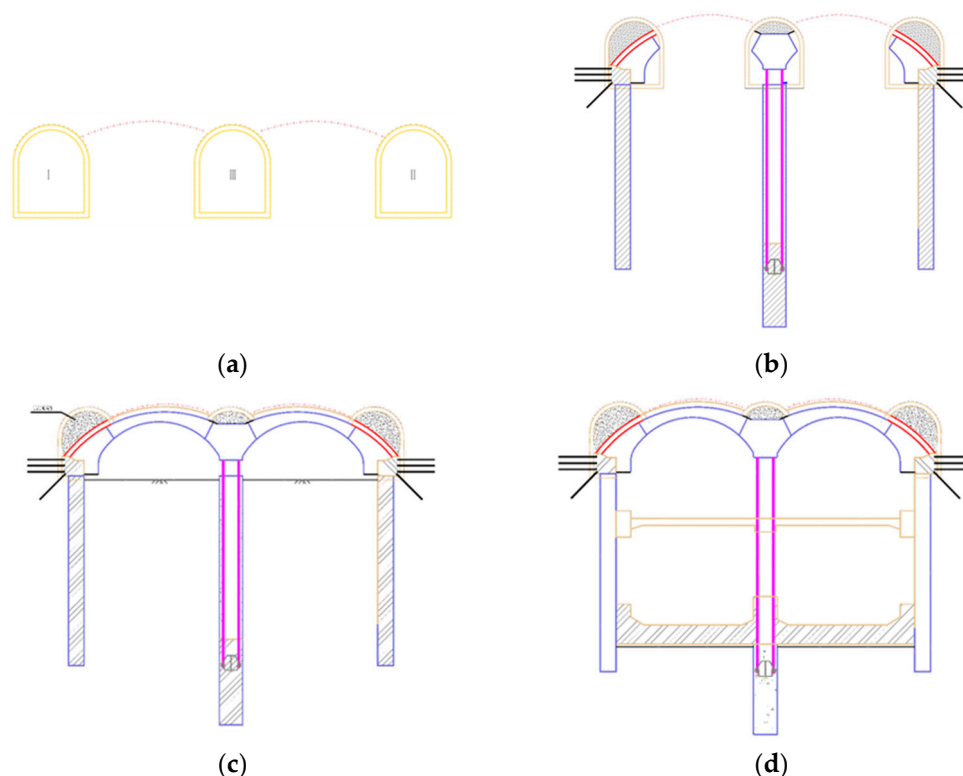


Figure 1. Construction process (a) Construction of the pilot tunnel; (b) Construction of pile beam; (c) Construction of the top arch; (d) Main body construction.

2.2. Engineering Geology

The geological distribution within the station is relatively complex, consisting top to bottom mainly of miscellaneous fill, residual soil (5N-1), residual soil (5N-2), castic rock, fine Sandstone, and conglomerate rock. However, the nature of the soil varies greatly from east to west, and the geological distribution at the east and west ends is not the same. Therefore, in order to study the influence of the rise–span ratio on the structure, the

geological parameters of the most unfavourable section that occurs during construction are selected as the parameters of this paper. To simplify the model, the thickness of the surrounding rock is simplified in this paper. The geological distribution is shown in Figure 2.

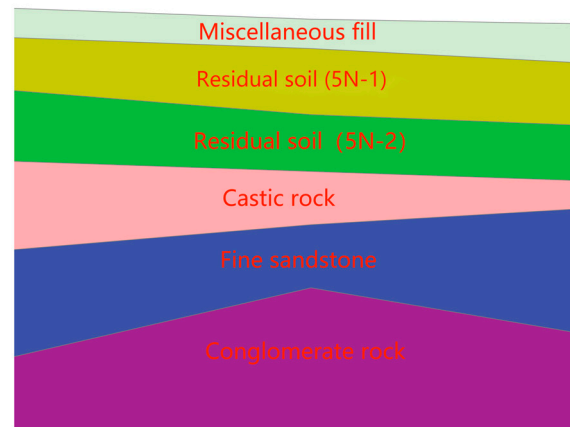


Figure 2. Geological distribution map.

2.3. Stress State of Arch Structure

The top arch structure of the pile–beam–arch method is simplified to a double arch symmetry model with steel pipe piles as the symmetry axis, as shown in Figure 3a. The upper arch structure is mainly subjected to overburden pressure and lateral soil pressure. The only loads considered in this structural model are the self-weight of the structure, the overburden and the lateral soil pressure, while bearing displacement, temperature change and other additional loads are not considered for the time being. The arch structure is considered as a linear elastic symmetrical structure with uniform material and is taken out separately for the force analysis. The upper arch structure is considered as a three-time super-stationary circular arc hinge-less arch structure with fixed supports, and the shallowly buried unbiased pressure model of the arch structure is shown in Figure 3b.

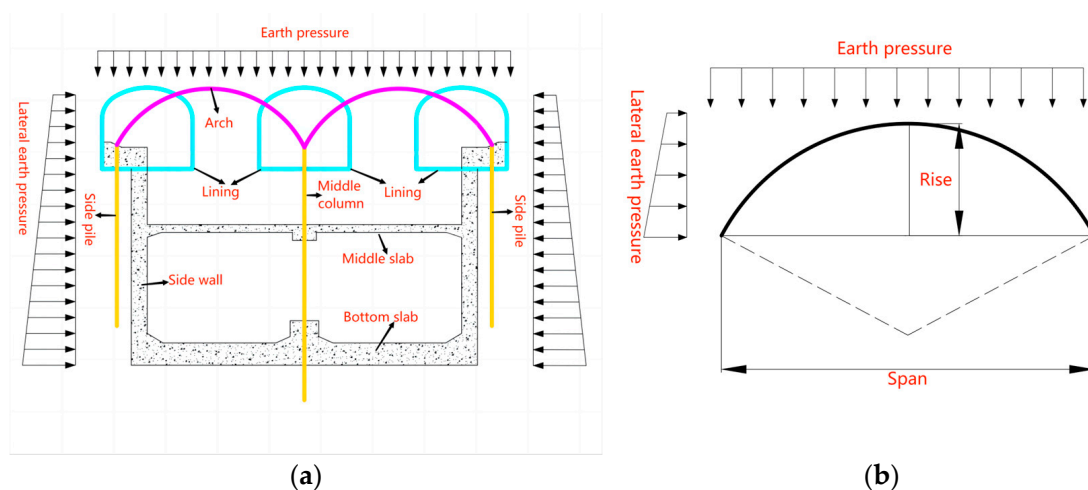


Figure 3. (a) Structure force sketch; (b) Basic load on the arch.

2.4. Surrounding Rock Pressure

The determination of the surrounding rock load acting on the support structure is an important aspect of the design of the tunnel load-structure method, and there are several representative calculation formulae: Terzaghi's theory [37], Bill Bowman's formula [38], and Xie Jiaxiao's formula [39]. Since most of the Chinese design units and Chinese codes

use Xie's formula for design and analysis, which is in accordance with Chinese production requirements, and the research station is located in Guangdong Province, China, this article also uses Xie's formula for load calculation. For shallowly buried unbiased tunnels, taking into account the surrounding rock, the load acting on the arch structure can be expressed as:

$$q = \gamma H \left(1 - \frac{H}{B_t} \lambda \tan \theta \right) \quad (1)$$

$$e_1 = \gamma H \lambda; e_2 = \gamma h \lambda \quad (2)$$

$$\lambda = \frac{\tan \beta - \tan \varphi_c}{\tan \beta [1 + \tan \beta (\tan \varphi_c - \tan \theta) + \tan \varphi_c \tan \theta]} \quad (3)$$

$$\tan \beta = \tan \varphi_c + \sqrt{\frac{(\tan^2 \varphi_c + 1) \tan \varphi_c}{\tan \varphi_c - \tan \theta}} \quad (4)$$

where γ is the weight of the surrounding rock (kN/m^2); H is the burial depth of the tunnel, referred to the distance from the top of the excavation to the ground (m); q is the average vertical pressure (kN/m^2); β is the angle between the fracture surface and the horizontal surface ($^\circ$); λ is the lateral pressure coefficient; h is the distance from the bottom of the pit to the horizontal surface; φ_c is the calculated angle of friction of the surrounding rock ($^\circ$); θ is the angle of friction on both sides of the soil column ($^\circ$).

3. Finite Element Analysis and Field Monitoring

The paper establishes a two-dimensional plane strain model applies the finite element software GTS NX, and uses the load-structure method to study the mechanical properties of steel pipe piles under different rise-span ratios. A three-dimensional finite element model is established to analyse the ground settlement control of the rise-span ratio.

3.1. Boundary Conditions and Basic Assumption

According to the theory of geomechanics [40], when the grid size is six times that of the excavated cavity, the influence of the soil in the construction excavation is relatively small. Therefore, the three-dimensional finite element model set up in this paper is the positive direction of the X axis horizontally to the right, the positive direction of the Y axis in the direction of the tunnel excavation, and the positive direction of the Z axis vertically from the surface upwards, with the dimensions of $X = 200$ m, $Y = 10$ m, and $Z = 70$ m, respectively, as shown in Figure 4.

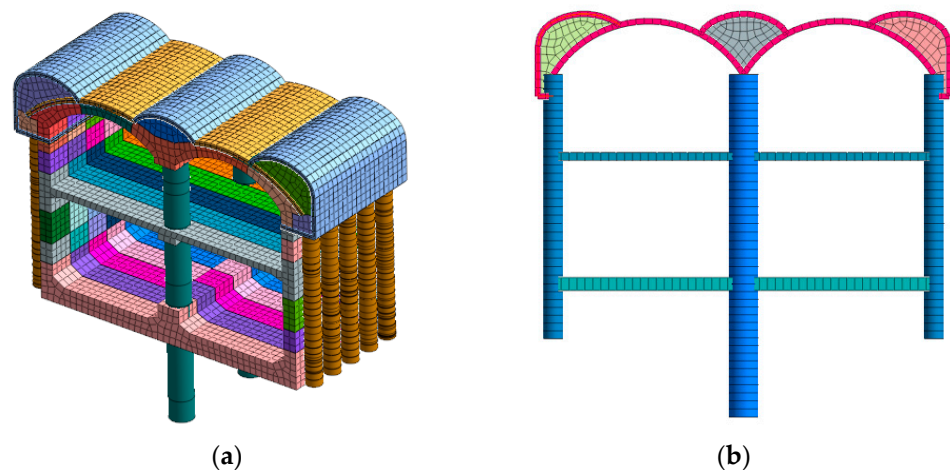


Figure 4. Finite element model diagram. (a) Stratum structure method; (b) loading-structure method.

The model boundary conditions are as follows: the top surface was free, the bottom surface was normally constrained and the outer boundary surface of the surrounding rock was normal to the vertical rock face.

Basic assumptions:

- Precipitation has been treated during construction, so the influence of ground water on the model is not considered.
- The station is a shallow tunnel excavation where only the weight load is considered. The soil constitutive model adopts the modified Mohr–Coulomb constitutive model and the concrete adopts the elastic constitutive model.
- The calculation model considers the formation material to be isotropic and homogeneous.
- The three-dimensional soil layer adopts the solid element, the lining adopts plate element and the pile adopts beam element. The two-dimensional soil layer adopts plane strain element, the lining adopts the beam element, and the pile adopts the beam element.

3.2. Model Parameters

The soil thickness of the layer has been adjusted according to the needs of the site as well as the actual numerical simulation. The soil properties of 5N-1 and 5N-2 are similar, so to simplify the soil layer and make it easier to set up the model, the two soil layers are merged. The mechanical parameters of the soil layer obtained by the survey unit in the field test and indoor geotechnical test are shown in Table 1.

Table 1. Physical and mechanical parameters.

Name of Soil Structure	Miscellaneous Fill	Residual Soil	Castic Rock	Fine Sandstone	Conglomerate Rock	C25 Lining	C35 Beam	C50 Steel Pipe Piles
Thickness H (m)	3	13	7	9	38	/	/	/
Poisson's ratio	0.4	0.35	0.3	0.3	0.25	0.25	0.2	0.2
Volumetric weight (kN/m ³)	19.5	20	20.5	25	25	25	25	25
Cohesion (kpa)	13	23	26	45	/	/	/	/
Internal friction angle (β)	14	25	28	30	/	/	/	/
E ₅₀ ^{ref} (Mpa)	4.536	5.184	8.856	12.96	/	/	/	/
E _{oed} ^{ref} (Mpa)	3.78	4.32	7.38	10.8	/	/	/	/
E _{ur} ^{ref} (Mpa)	26.46	30.24	51.66	75.6	/	/	/	/
E (Mpa)	/	/	/	/	8000	30,000	32,000	35,000

where: E₅₀^{ref}, secant elastic modulus in shear hardening; E_{oed}^{ref}, secant elastic modulus in shear hardening; E_{ur}^{ref}, elastic modulus at unloading; E, elastic modulus.

In the construction of the pilot tunnel, the lining is reinforced concrete consisting of concrete and steel grids to resist the stresses released by the excavation, maintain the stability of the excavation surface and prevent the tunnel from collapsing. In the finite element model, the equivalent stiffness method [41] was usually used to treat the steel grid as equivalent, and the steel grid was converted to the elastic modulus of the concrete. The elastic of elasticity of the lining after conversion:

$$E = E_0 + \frac{A_g \cdot E_g}{A_c} \quad (5)$$

where, E: elastic modulus of concrete after conversion; E₀: original elastic modulus of concrete; E_g: elastic modulus of steel grid; A_g: cross-sectional area of the steel grid; A_c: cross-sectional area of concrete.

The pile and the surrounding soil will have a tangential slip tendency and a normal separation tendency. Therefore, the role of soil–structure interaction in finite element numerical simulation cannot be ignored in this study. In the GTS NX software(2021R1,MIDAS Information Technology Co., Ltd., Beijing, China), the pile element is composed of a beam element and a contact element, and the contact element represents the pile–soil contact

relationship. The contact element consists of a tangential spring and a normal spring. The values of normal modulus K_n and tangential modulus K_t can be obtained by two-dimensional plane strain in the GTS NX software. K_s is the spring factor of the foundation, which can be derived from field tests. The schematic diagram of the pile interface contact element is shown in Figure 5.

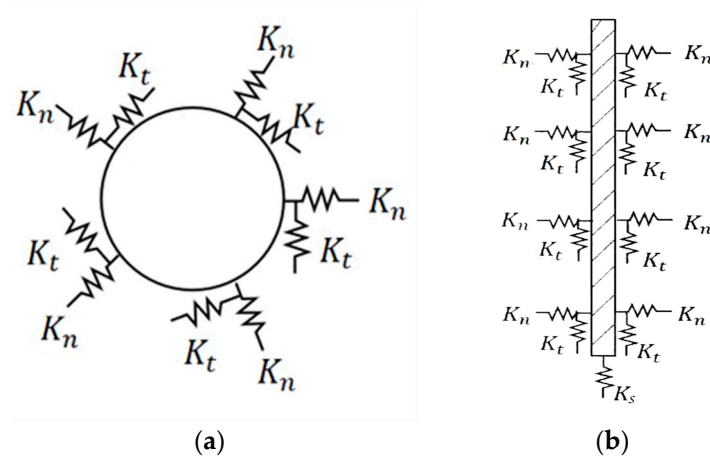


Figure 5. Pile element contact model diagram: (a) horizontal direction; (b) cutaway drawing.

3.3. Construction Stage

According to the definition of the rise–span ratio, it is known that the rise–span ratio is the ratio of the height to the calculated span diameter. According to the design data of this subway station, the rise–span ratios of the pile–beam–arch method are set to 0.22, 0.25, 0.28, 0.31, 0.34, and 0.37, respectively, and the two-dimensional finite element model and the three-dimensional finite element model are established to study the force characteristics and soil surface deformation of the structure at each construction stage, with other conditions unchanged. The expression of rise–span ratio is as follows:

$$\mu = \frac{r}{s} \quad (6)$$

where, μ is the rise–span ratio, r is the height, and s is the span.

The construction stages of the three-dimensional finite element model correspond to the real construction stages. The simulation of the construction stages is carried out according to the following process: pilot tunnel (lining) → centre pile and side pile (simultaneously providing pile interface unit and pile end unit) → longitudinal beam → arch structure (lining) → pilot tunnel backfill → B1 layer excavation → B2 layer excavation. The excavation part chooses the passivation treatment and the structure to be added chooses the activation treatment. In the model, concrete activation is simulated by changing the properties of the original soil.

3.4. Distribution of Monitoring Points

During the excavation of the pilot tunnel, a number of settlement monitoring points are placed on the surface, one every 15 m in the longitudinal direction, and the horizontal distribution monitoring is shown in Figure 6.

The soil settlement monitoring points should penetrate the hard shell layer, and should be separated from the hard shell layer and in close contact with the original soil under the hard shell layer, and it is strictly forbidden to take the shallow way to set up the monitoring points. The monitoring point is installed by drilling through the hard crustal layer with a 150 mm diameter water auger and then burying the measuring rod in the soil layer, protected to the ground by a casing filled with medium coarse sand and cement mortar between the casing and the borehole. The measuring rod was not less than $\Phi 16$, length of not less than 800 mm. the top of the measuring point from the bottom of the protective

cover of about 30 mm. The distribution points for monitoring settlement maxima during construction on site are shown in Figure 7.

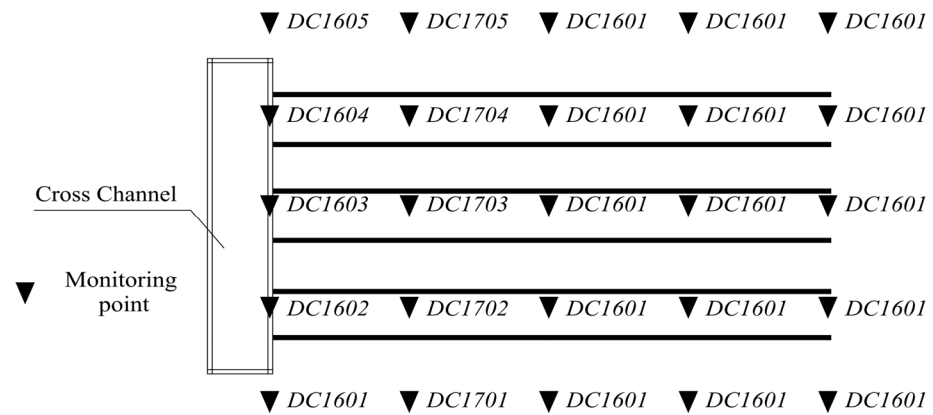


Figure 6. Distribution of surface subsidence observation.

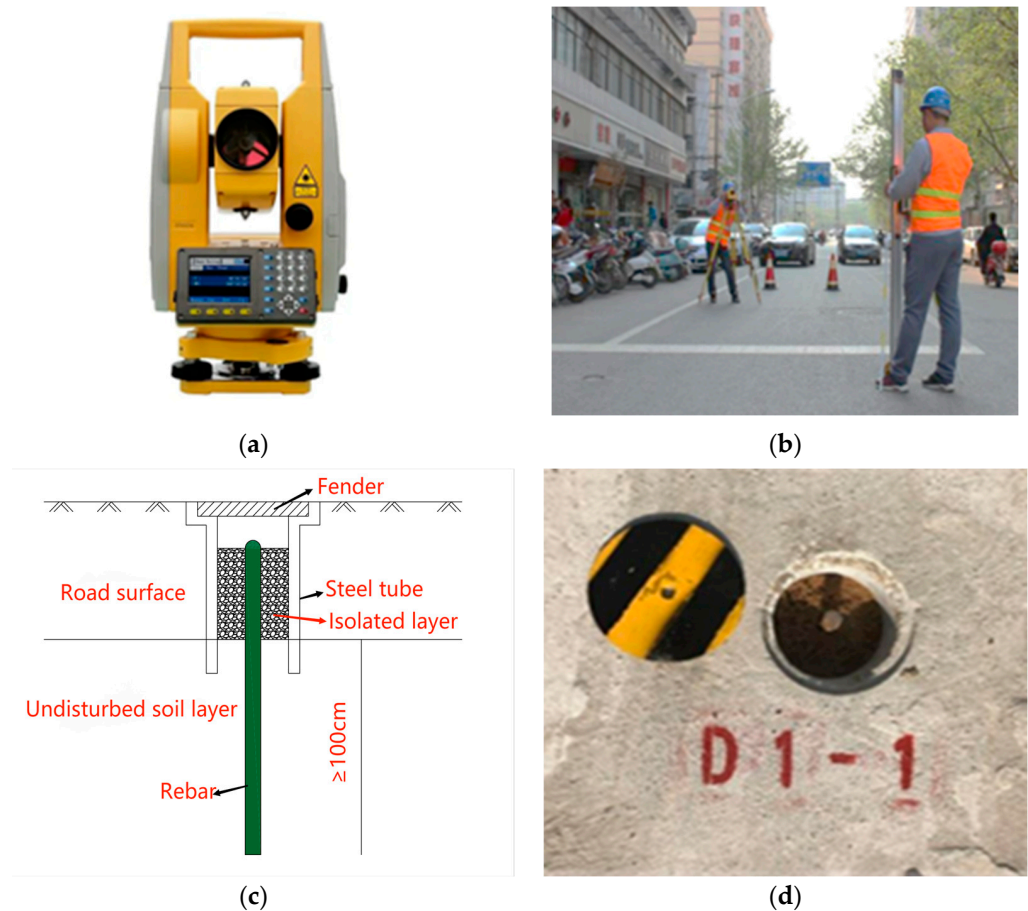


Figure 7. Monitoring schematic diagram. (a) Total Station. (b) Observation point. (c) Observation point profile. (d) Overhead view of the observation point.

4. Result Analysis

4.1. Ground Surface Settlement Analysis

After the finite element calculation of the pile–beam–arch method model for the six conditions of the rise–span ratios, the variation in displacement for each construction phase can be solved. The variation in ground surface settlement is shown in Figure 8.

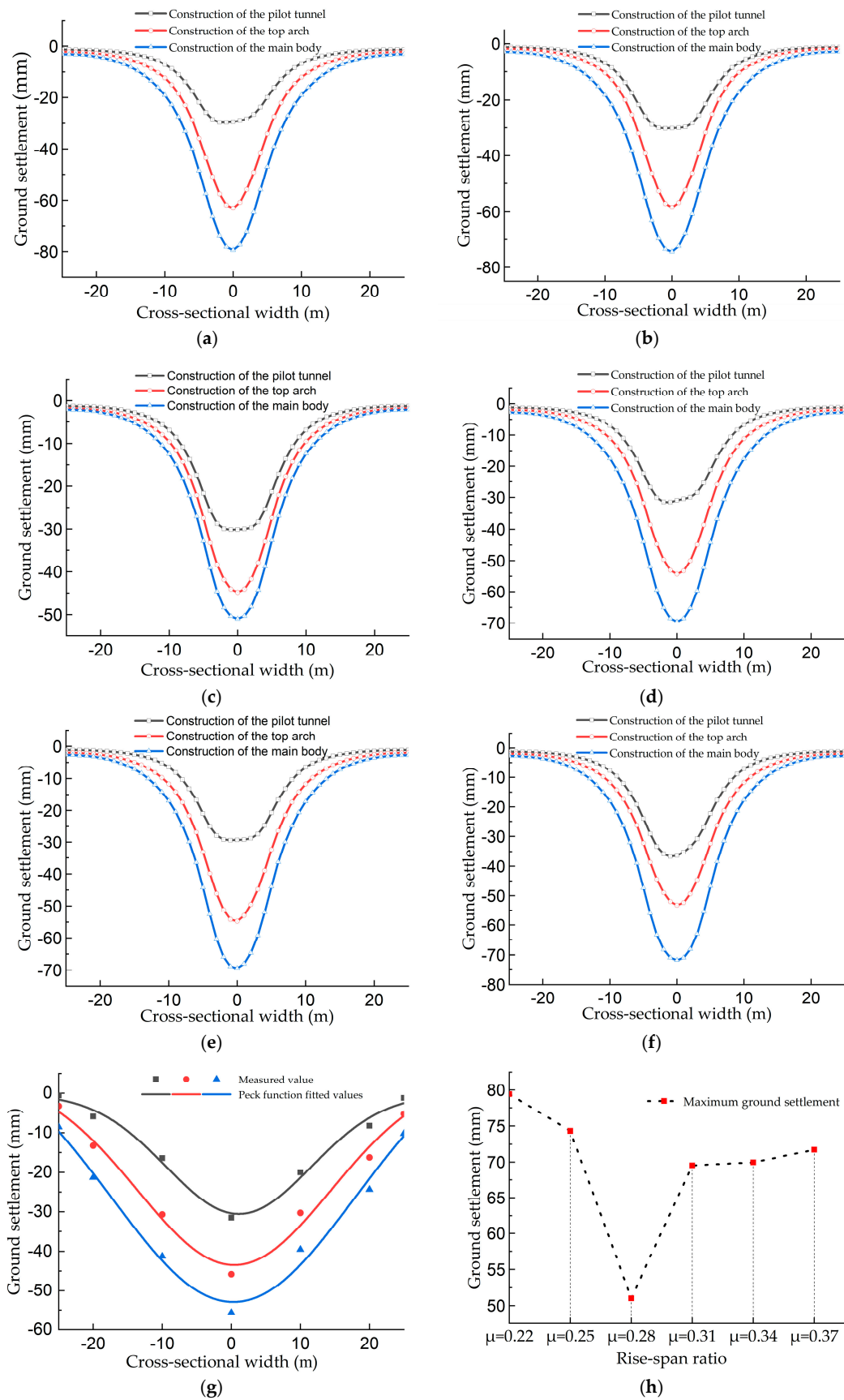


Figure 8. (a) $\mu = 0.22$; (b) $\mu = 0.25$; (c) $\mu = 0.28$; (d) $\mu = 0.31$; (e) $\mu = 0.34$; (f) $\mu = 0.37$; (g) Cross-sectional field monitoring; (h) Max settlement values for each rise-span ratios.

The pile–beam–arch method with six kinds of rise–span ratios can be solved to obtain the displacement variation in each construction stage after finite element calculation. Since the settlement hardly changes in the beam–pile construction phase, the settlement values of the beam–column construction are not shown in the Figure 8. The variation in settlement is shown in Figure 8.

Different rise–span ratios have a significant effect on surface settlement, and when the rise–span ratio is 0.22, the maximum value of surface settlement is approximately 79 mm. When the rise–span ratio is 0.28, the surface settlement is reduced 51 mm, and the difference between the two is 28 mm, a reduction of 35%. The actual rise–span ratio of the station is between 0.28 and 0.31. From Figure 8g, it can be concluded that the change law of the surface settlement of the simulated value and the monitoring value is approximately the same, which confirms the accuracy of the finite element numerical simulation from the side. Due to the effect of stress redistribution, it leads to the displacement of the soil in the borehole and eventually forms loosening. From the analysis of the measured data, the surface settlement caused by the excavation of the cave pile method and the settlement trough theory proposed by the Peck curve have some agreement. The width of the settlement trough decreases with increasing depth of burial, so that the settlement of the vault caused by the excavation of the station is not completely transferred to the surface, and the self-stability and stress redistribution of the soil will absorb part of the deformation, reflecting the process that the deep soil disturbance is gradually transferred to the surface in an expanding trend.

From Figure 8 it can be seen that the settlement is greater when the rise–span ratio is relatively small. However, this does not mean that the settlement becomes smaller as the rise–span ratio increases. When the rise–span ratio is 0.28, the settlement reaches the minimum value. As the rise–span ratio increases, the settlement increases and the overall trend is first to decrease and then to increase. However, after the rise–span ratio of 0.28, although the settlement volume becomes larger, the increase is more moderate and almost no change occurs, and the settlement volume tends to a stable state.

The amount of surface settlement caused by the four main construction stages of the pile–beam–arch method is shown in Table 2.

Table 2. Percentage of ground settlement at each construction stage.

Stage	Pilot Tunnel	Beam and Column	Top Arch	Main Body
$\mu = 0.22$	37.03%	4.83%	37.58%	20.56%
$\mu = 0.25$	40.51%	5.06%	33.04%	21.39%
$\mu = 0.28$	59.00%	6.15%	22.67%	12.17%
$\mu = 0.31$	44.27%	5.31%	29.65%	20.78%
$\mu = 0.34$	42.12%	5.58%	30.65%	21.64%
$\mu = 0.37$	42.28%	4.20%	28.39%	25.13%

It can also be seen from Table 2 that each rise–span ratio accounts for more than 37–59% of the total settlement in the pilot tunnel construction stage, about 5% for the pile–beam column, 20–37% for the top arch construction, and 12–20% for the main construction. The rise–span ratio of each of the first two construction stages is basically the same, and all the influencing factors have not changed, so it is basically maintained at about 30 mm, which is also close to the measured value. In the article, by studying the rise–span ratio of the top arch, there is a significant difference in the surface settlement caused by the top arch construction stages at different rise–span ratios. At the rise–span ratio of 0.28, the settlement caused by the top arch construction is only 11.57 mm, accounting for about 22.67% of the total settlement, which is obviously smaller than the settlement caused by the top arch construction under other rise–span ratio, so the reasonably designed rise–span ratio can effectively control the ground surface settlement and help to protect a series of civil facilities such as underground pipelines.

When the rise–span ratio is 0.28, the construction phase of the guide tunnel group (i.e., the first construction phase) and the construction phase of the top arch (i.e., the third construction phase) are the two main phases of settlement growth, and the settlement of these two phases accounts for approximately 81.67% of the settlement of the entire construction process, which indicates that a reasonable rise–span ratio can increase the resistance of the arch, which is conducive to the stability of the entire structure and the mechanical system of the structure. The lower the settlement caused by the main structure, the more favourable it is for the subsequent construction of the large excavation area. The top arch rise–span ratios of 0.22, 0.25, 0.28, 0.31, 0.34, and 0.37 show a trend of decreasing and then increasing settlement in the construction of the top arch, which also indicates that the top arch rise–span ratio needs to be set at a reasonable range.

From Figure 9, it can be seen that the measured and simulated values have the same trend, and the actual design of each rise–span is between 0.28 and 0.31, because the finite element calculation does not consider the dynamic load and groundwater, which leads to the error between the simulated and measured values. However, the measured values and the rise–span ratio of 0.22 or 0.31 are basically the same, and the larger and smaller rise–span ratios increase the settlement caused by the construction, which also proves that a reasonable design of the rise–span ratio can control the settlement of the ground surface.

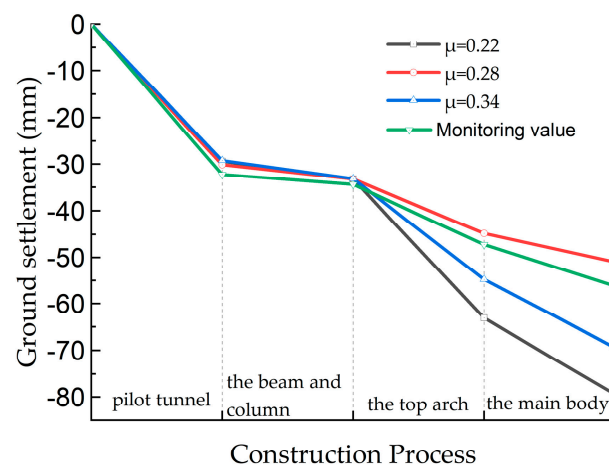


Figure 9. Comparison of measured and simulated values.

4.2. Force Characteristics of Each Rise–Span Ratios

The buckled arch is an important part of the pile–beam–arch method station structure, its function is to form the upper support arch so that the frame support system is complete and the upper surrounding rock load is transferred to the infill pile. However, during the construction of the buckled arch, the stability of the surrounding rock will be affected and the mechanical properties will be reduced due to the construction of the guide cavern, which will increase the risk of collapse of the arch, and therefore the buckled arch construction is a dangerous part of the construction.

4.2.1. Steel Pipe Pile Axial Force Analysis

The article uses the finite element analysis method to calculate the mechanical properties of the vault at different each rise–span ratio, and the two-dimensional finite element model to analyse the internal force characteristics of the steel pipe piles. The relationship between the maximum axial force and the rise–span ratio of steel pipe piles is shown in Figure 10. The axial force accumulation of different rise–span ratios in the main stages of the pile is shown in Figure 11.

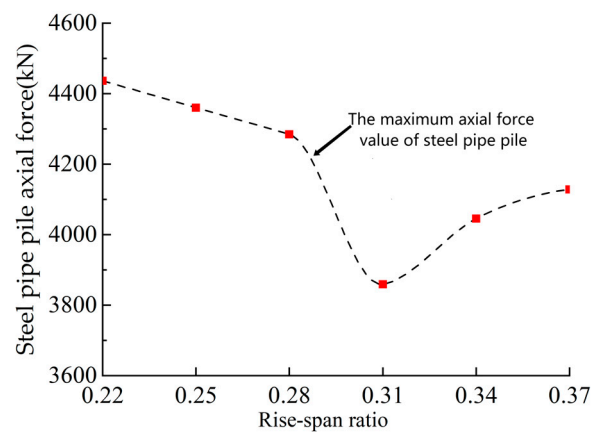


Figure 10. Max axial force of steel pipe piles with each the rise–span ratio.

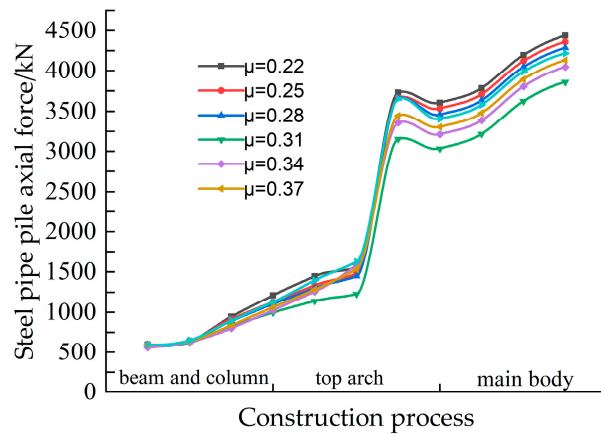


Figure 11. Steel pipe pile axial force diagram.

The axial force of the steel pipe pile is plotted from the finite element model. It can be seen from Figure 10 that the maximum axial force of the centre pile for each rise–span ratio, as a whole, tends to first decrease and then increase with the increase in rise–span ratio, at a rise–span ratio of 0.22, the axial force of the centre pile is 4430 kN, and at a rise–span ratio of 0.31, the maximum axial force of the centre pile is 3860 kN, a decrease of 13% of the peak value. From the longitudinal comparison in Figure 11, it can be seen that in the top arch stage, as the top arch construction progresses, the excavation area of the soil between the pilot tunnels will increase and the internal cavity area will increase, the overburden pressure will be transferred to the centre pile and the side piles, at this time, the centre pile and the construction of the top and bottom longitudinal beams will form a stable frame structure to jointly bear the force, and the force of the centre pile will start to be prominent, so the axial force of the centre pile will increase sharply. The process of mechanical transformation of the cavity pile method is achieved. The sudden increase in axial force of the centre pile is the result of the excavation of the soil between the pilot tunnels, and the overburden pressure is transferred to the centre pile. After partial removal of the initial support in the pilot tunnels, the axial force in the centre pile was slightly reduced by the addition of cross bracing to ensure the stability of the structure as required by the design, taking into account the stiffness of the structure. However, as construction progressed, the axial force in the centre pile continued to increase until it reached its maximum value.

4.2.2. Analysis of Axial Forces in the Top Arch

The variation in the axial force for each rise–span ratios are derived from the FEA software (2021R1, MIDAS Information Technology Co., Ltd., Beijing, China), as shown in Figures 12–14.

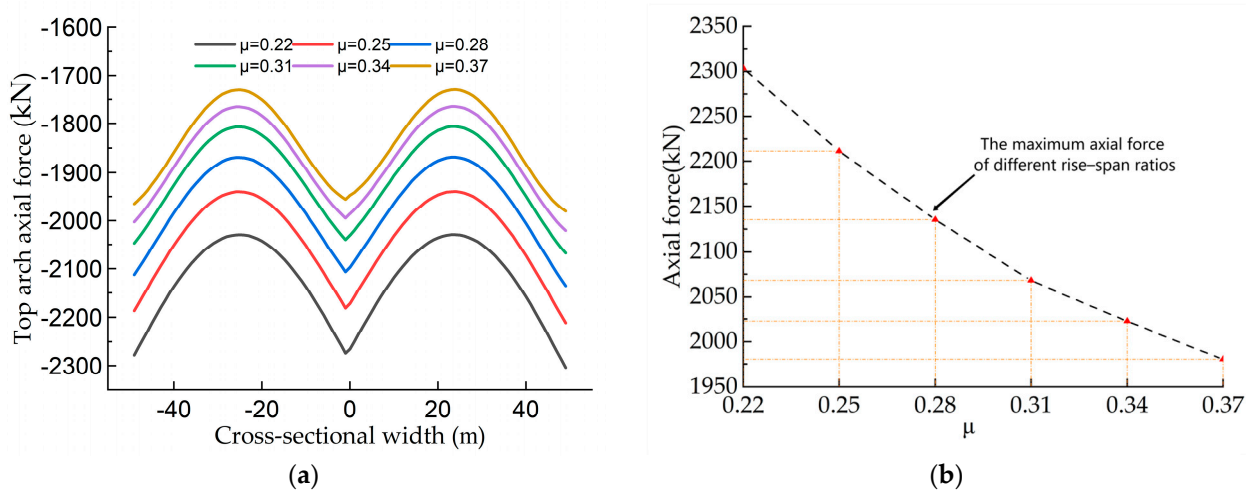


Figure 12. (a) Cross-sectional the top arch axial force diagram; (b) Maximum axial force values for each rise–span ratios.

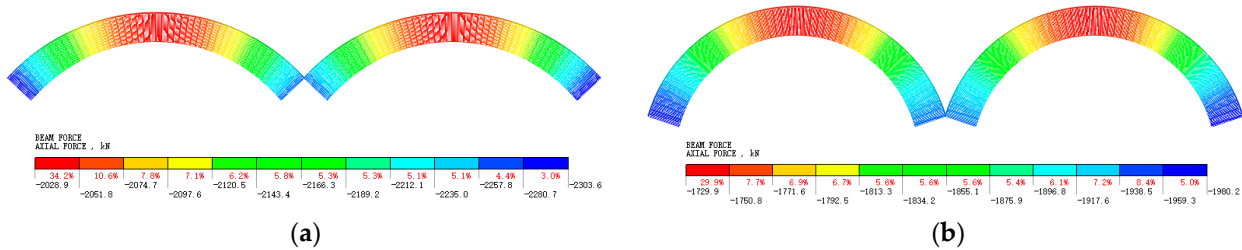


Figure 13. (a) Axial force cloud map ($\mu = 0.22$); (b) $\mu = 0.37$ Axial force cloud map ($\mu = 0.37$).

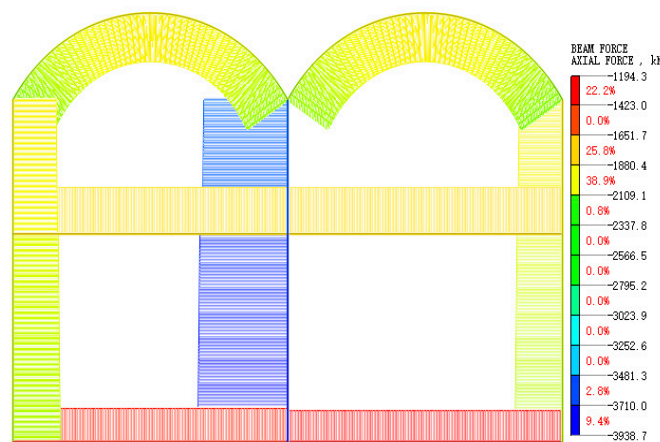


Figure 14. Axial forces for each rise–span ratios ($\mu = 0.28$).

The variation in the top arch axial force for each rise–span ratios is shown in Figures 12 and 13. The variation in the axial force of the top arch in the cross-section is similar to the shape of an “arch”. The axial force of the top arch is negatively correlated with the rise–span ratio, and the axial force of the top arch gradually decreases as the

rise–span ratio increases, and the rate of decrease is also decreasing, tending to converge. The maximum axial force value of the arch structure decreases from 2303.6 kN at $\mu = 0.22$ to 1982.1 kN at $\mu = 0.37$, a reduction of 14% of the maximum axial force value. An excerpt from the axial force clouds for a rise–span ratio of 0.22 and a rise–span ratio of 0.37 shows that the maximum axial force in the arch occurs at the foot of the arch and the minimum axial force at the top of the arch, and that the axial force in the central arch is slightly less than that in the two side arches. The axial force cloud of the overall structure (Figure 14) shows that the maximum axial force is at the junction of the steel pipe piles and the base plate, and the axial force of the steel pipe piles is greater than that of the side piles.

4.2.3. Analysis of the Bending Moment in the Top Arch

The variation in the bending moment for each rise–span ratio is derived from the FEA software, as shown in Figures 15–17.

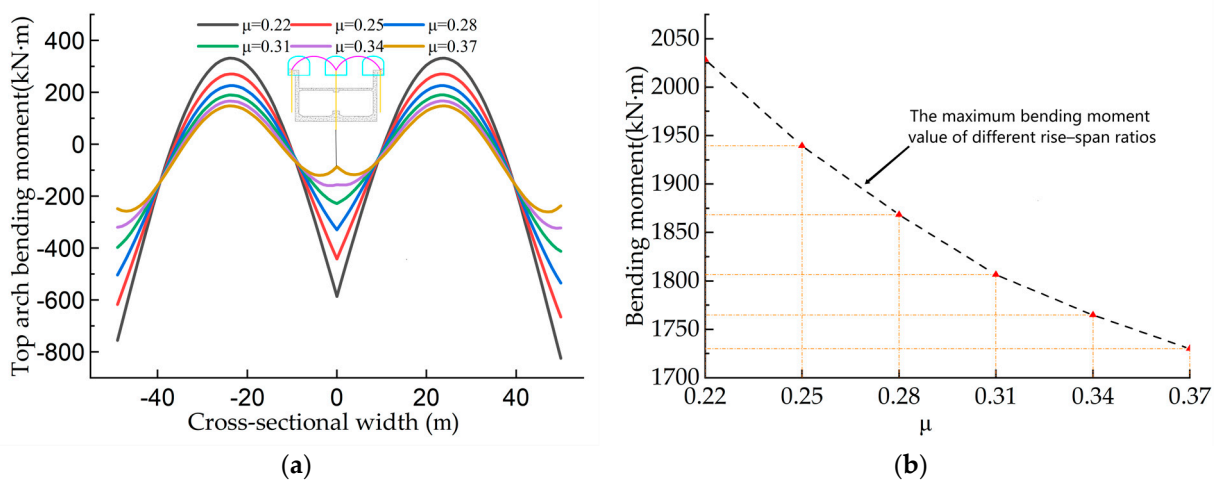


Figure 15. (a) Cross-sectional the top arch bending moment diagram; (b) Maximum bending moment values for each rise–span ratios.

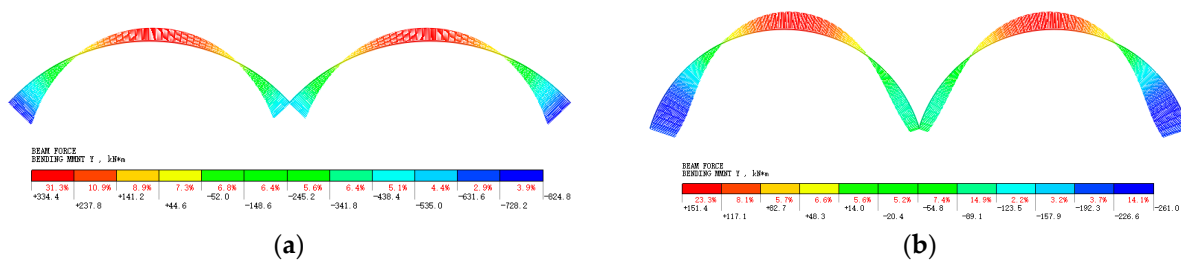


Figure 16. (a) Bending moment cloud map ($\mu = 0.22$); (b) Bending moment cloud map ($\mu = 0.37$).

The bending moment at the top of the arch varies as shown in Figures 15 and 16. The maximum value of the bending moment occurs at the foot of the arch, the bending moment at the top of the arch and the bending moment at the foot of the arch have opposite directions, and the bending moment at the shoulder of the arch has the smallest value. From Figure 15, it can be seen that the bending moment at the top of the arch and the rise–span ratio are negatively correlated, and as the rise–span ratio increases, the maximum axial force at the top of the arch decreases, and the drop also decreases, tending to converge. The maximum moment value of the arch structure decreases from 824.85 (kN·m) at $\mu = 0.22$ to 261 (kN·m) at $\mu = 0.27$, a reduction of 68% of the maximum moment value. The rise–span ratio has a relatively greater effect on the bending moment than the axial force. The overall bending moment cloud is shown in Figure 17. In terms of the overall structural analysis,

the larger bending moments are found at the joints between the floor slab and the side and centre piles.

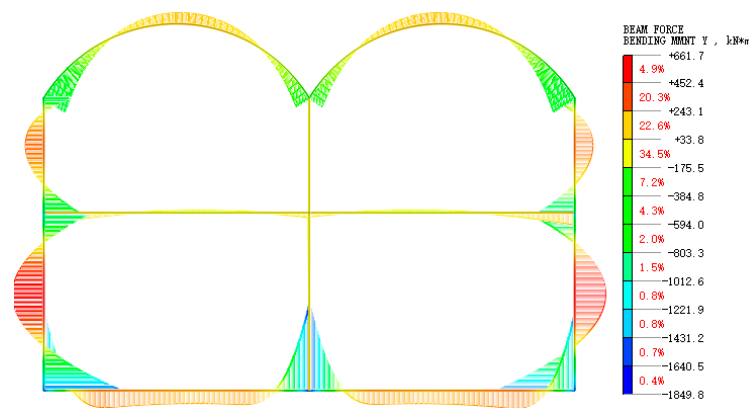


Figure 17. Bending moment for each rise–span ratios ($\mu = 0.28$).

5. Discussion

The pile–beam–arch method is a construction form that combines the shallow-buried excavation method and the cover excavation method. It allows vehicles to drive on the upper pavement, which inevitably leads to the influence of dynamic load on soil excavation. However, this paper ignores the influence of the upper dynamic load on the construction of the pile–tunnel method. The next work can refer to R.V. Goldstein’s research results of using the modified Cam-clay (MCC) constitutive model under dynamic load conditions to conduct a further comprehensive study of the surface settlement of the pile–beam–arch method [42].

The hole pile subway construction technology is the first application in South China, and the opposite soft layer is relatively thick. This research can provide engineering experience for the wider promotion of the hole pile method in South China in the future. In this paper, the influence of the rise–span ratio on the surface settlement and the steel pipe pile in the construction process of the hole–pile method is investigated by three-dimensional finite element modelling and on-site monitoring. Through this study, the settlement law of the hole–pile method in the weak layer in southern China is found, which fills the research gap in the construction technology of the hole–pile in southern China. The maximum surface settlement ($\mu = 0.31$) calculated by the finite element method is about 59 mm, which is different from the maximum settlement value of 30 mm mentioned by Xiangyu Guo [23]. The thickness of the weak layer of the subway station in this paper is relatively large, the bearing capacity of the foundation is obviously weak, and the hole pile method in this paper belongs to the semi-reverse construction method and Guo’s reverse construction method. There are differences, which may be the cause of different surface settlement. At the same time, B. Li’s article also shows that, in fact, in the actual monitoring, it can be concluded that the surface settlement caused by the excavation of the hole pile method is often much larger than the standard value [43].

In this finite element modelling analysis, the pilot tunnel stage and the buckle arch stage were found to be the main stages of surface settlement. This result is consistent with the field monitoring data of 30 Beijing subways summarised by Yu [20]. However, the sum of the pilot tunnel stage and the arch stage accounts for about 80% of the total settlement, which is 10% less than that of Yu [20], due to the neglected interaction between the pilot tunnel lining and the soil structure. The pit–pile method has inevitable advantages in the construction of underground stations and will certainly be used in more areas in the future. The relatively stable soil layer still causes relatively large settlements, especially in the weak layer, so it is necessary to reinforce the layer in advance, for example by using high-pressure jet grouting piles [44].

6. Conclusions

The paper establishes a finite element model, verifies the accuracy of the finite element simulation values of the rise–span ratio based on the monitoring data collected at the site, and analyses the internal force trends of the steel pipe piles and the top arch structure and the ground settlement control under different rise–span ratios by setting different rise–span ratios of the vault. The main conclusions are:

- (1) Different rise–span ratios have different responses to the ground settlement caused by the construction of cavity pile method metro stations. The ground settlement first decreases and then increases with increasing rise–span ratio, but the rate of increase becomes smaller and tends to converge. The rise–span ratio of 0.28 has the lowest settlement, which is 22 mm less than the maximum value and accounts for 27% of the maximum settlement. By setting a reasonable rise–span ratio, the amount of surface settlement caused by excavation of the section can be effectively controlled.
- (2) According to the field monitoring data and finite element model analysis, the surface settlement caused by the construction of the pilot tunnels accounted for at least 50% of the total settlement, and the excavation of the pilot tunnels was the main construction stage leading to the surface settlement. The cross-sectional settlement curve shows a symmetrical distribution on both sides of the station. The settlement caused by the main construction with a rise–span ratio of 0.28 is significantly reduced, increasing the stiffness and strength of the structure and facilitating the excavation of large sections during the main construction.
- (3) The different rise–span ratios of the pile–beam–arch method have a greater impact on the internal forces of the structure. The maximum axial force of steel pipe pile with different rise–span ratio is parabolically distributed, large on both sides and small in the middle, the axial force of the middle pile increases continuously with the construction, and the axial force of the middle pile is the smallest when the rise–span ratio is 0.31. The maximum axial force and the maximum bending moment of the vault are negatively correlated with the rise–span ratio.
- (4) Combined with the analysis of the internal force characteristics of the pile–beam–arch method structure and the ground settlement control, the arch structure and the pilot tunnels structure are located in the ground with weak foundation bearing capacity such as residual soil. If the rise–span ratio is too high, the shear force of the arch will be reduced and the horizontal shear force will be greater, resulting in difficulties in the construction at the foot of the arch; if the rise–span ratio is designed to be 0.28–0.31, the stability of the station structure and the deformation of the ground surface will be better ensured.

Author Contributions: Conceptualization, J.L. (Jianbing Lv) and J.L. (Jianjun Lu); methodology, H.W.; software, H.W. and J.L. (Jianjun Lu); validation, H.W. and J.L. (Jianjun Lu); formal analysis, J.L. (Jianjun Lu); investigation, J.L. (Jianjun Lu); resources, J.L. (Jianbing Lv); data curation, J.L. (Jianbing Lv); writing—original draft preparation, J.L. (Jianjun Lu); writing—review and editing, J.L. (Jianbing Lv). All authors have read and agreed to the published version of the manuscript.

Funding: Foundation of Outstanding Youth of Guangdong Province—Research on Bearing Mechanism and Stability of pile foundation in Karst Area based on static and dynamic loads and time-varying soil Characteristics, (Approval number: 2023B1515020061).

Institutional Review Board Statement: Not applicable.

Informed Consent Statement: Not applicable.

Data Availability Statement: Not applicable.

Acknowledgments: The authors wish to express their gratitude to the reviewers and editors for their positive and constructive comments and suggestions on the manuscript.

Conflicts of Interest: The authors declare no conflict of interest.

References

1. Koutsoftas, D.C.; Frobenius, P.; Wu, C.L.; Meyersohn, D.; Kulesza, R. Deformations during cut-and-cover construction of Muni Metro Turnback project. *J. Geotech. Geoenviron. Eng.* **2000**, *126*, 344–359. [[CrossRef](#)]
2. Liu, W.; Luo, F.; Mei, J. A new construction method for a metro station in Beijing. *Tunn. Undergr. Space Technol.* **2000**, *15*, 409–413. [[CrossRef](#)]
3. Zhao, K.; Hao, Z.; Luo, F.; Li, S. A New Construction Method for Deeply Buried Metro Station in Rich Water Strata. In Proceedings of the 2015 3rd International Conference on Advances in Energy and Environmental Science, Zhuhai, China, 25–26 July 2015; Atlantis Press: Amsterdam, The Netherlands, 2015.
4. Luo, F.; Wang, Y. Analysis on Ground Surface Deformation of Mined Metro Station Constructed by PBA Method in Beijing. *Tunn. Constr.* **2016**, *36*, 20.
5. Fang, Q.; Zhang, D.; Wong, L.N.Y. Shallow tunnelling method (STM) for subway station construction in soft ground. *Tunn. Undergr. Space Technol.* **2012**, *29*, 10–30. [[CrossRef](#)]
6. Cherlo, M.A.; Hashemolhosseini, H.; Cheraghi, M.; Mahdevari, S. Feasibility evaluation for excavation of Naghshe Jahan Square subway station by underground methods. *J. Rock Mech. Geotech. Eng.* **2013**, *5*, 452–459. [[CrossRef](#)]
7. Sadaghiani, M.H.; Dadizadeh, S. Study on the effect of a new construction method for a large span metro underground station in Tabriz-Iran. *Tunn. Undergr. Space Technol.* **2010**, *25*, 63–69. [[CrossRef](#)]
8. Liu, X.; Liu, Y.; Yang, Z.; He, C. Numerical analysis on the mechanical performance of supporting structures and ground settlement characteristics in construction process of subway station built by Pile-Beam-Arch method. *KSCE J. Civ. Eng.* **2017**, *21*, 1690–1705. [[CrossRef](#)]
9. Chakeri, H.; Ozelik, Y.; Unver, B. Effects of important factors on surface settlement prediction for metro tunnel excavated by EPB. *Tunn. Undergr. Space Technol.* **2013**, *36*, 14–23. [[CrossRef](#)]
10. Liu, X.; Liu, Y.; Qu, W.; Tu, Y. Internal force calculation and supporting parameters sensitivity analysis of side piles in the subway station excavated by Pile-Beam-Arch method. *Tunn. Undergr. Space Technol.* **2016**, *56*, 186–201. [[CrossRef](#)]
11. Ocak, I. Control of surface settlements with umbrella arch method in second stage excavations of Istanbul Metro. *Tunn. Undergr. Space Technol.* **2008**, *23*, 674–681. [[CrossRef](#)]
12. Guo, X.; Jiang, A. Study on the stability of a large-span subway station constructed by combining with the shaft and arch cover method. *Tunn. Undergr. Space Technol.* **2022**, *127*, 104582. [[CrossRef](#)]
13. Li, S.; Zhang, Y.; Cao, M.; Wang, Z. Study on excavation sequence of pilot tunnels for a rectangular tunnel using numerical simulation and field monitoring method. *Rock Mech. Rock Eng.* **2022**, *55*, 3507–3523. [[CrossRef](#)]
14. Dindarloo, S.R.; Siami-Irdemoosa, E. Maximum surface settlement based classification of shallow tunnels in soft ground. *Tunn. Undergr. Space Technol.* **2015**, *49*, 320–327. [[CrossRef](#)]
15. Jeon, S.; Kim, J.; Seo, Y.; Hong, C. Effect of a fault and weak plane on the stability of a tunnel in rock—A scaled model test and numerical analysis. *Int. J. Rock Mech. Min. Sci.* **2004**, *41*, 658–663. [[CrossRef](#)]
16. Li, T.; Zhang, Z.; Luo, M.; Liu, B.; Wang, Y.; Li, L. Analytical Solution of Loosening Pressure Model for Shallow Tunnel Based on Pile-Beam-Arch Method. *KSCE J. Civ. Eng.* **2022**, *26*, 3648–3662. [[CrossRef](#)]
17. Ding, D.Y.; Yang, X.R.; Lu, W.; Liu, W.N.; Yan, M.; Li, A.M. Numerical Analysis of Metro Station Construction by Large-Diameter Shield and Pile-Beam-Arch Method. *Adv. Mater. Res.* **2011**, *368–373*, 2711–2715. [[CrossRef](#)]
18. Xu, F.; Li, L.; Zhang, Q.; Wang, Z.; He, P. Analysis on the Response of Ground Surface Settlement for a Metro Station during Construction Using the Pile-Beam-Arch (PBA) Method Subjected to Pore Pressure. *Geo-China* **2016**, *2016*, 243–250.
19. Liu, J.X.; Fang, W.; He, S.H.; Wang, E.; Zhou, H. Enlarging a large-diameter shield tunnel using the Pile-Beam-Arch method to create a metro station. *Tunn. Undergr. Space Technol.* **2015**, *49*, 130–143. [[CrossRef](#)]
20. Yu, L.; Zhang, D.; Fang, Q.; Cao, L.; Xu, T.; Li, Q. Research on Surface Settlement of Subway Station Construction Using Pile-Beam-Arch Approach. *IOP Conf. Ser. Earth Environ. Sci.* **2019**, *455*, 012167.
21. Zeng, Y.S.; Bai, Y.; Zou, Y.; Huang, B. Numerical Study on Stratigraphic and Structural Deformation Patterns Considering Surface Load with Pile-Beam-Arch Method Construction. *Symmetry* **2022**, *14*, 1892. [[CrossRef](#)]
22. Guan, Y.-P.; Zhao, W.; Li, S.-G.; Zhang, G.-B. Key techniques and risk management for the application of the Pile-Beam-Arch (PBA) excavation method: A case study of the Zhongjie subway station. *Sci. World J.* **2014**, *2014*, 275362. [[CrossRef](#)] [[PubMed](#)]
23. Guo, X.; Wang, Z.; Geng, P.; Chen, C.; Zhang, J. Ground surface settlement response to subway station construction activities using pile-beam-arch method. *Tunn. Undergr. Space Technol.* **2020**, *108*, 103729. [[CrossRef](#)]
24. Guo, X.; Jiang, A.; Wang, S. Study on the Applicability of an Improved Pile-Beam-Arch Method of Metro Station Construction in the Upper-Soft and Lower-Hard Stratum. *Adv. Civ. Eng.* **2021**, *2021*, 6615016. [[CrossRef](#)]
25. Peck, R.B. Deep excavations and tunnelling in soft ground. In Proceedings of the 7th International Conference on Soil Mechanics and Foundation Engineering, Mexico City, Mexico, 29 August 1969.
26. Litwiniyszyn, J. The theories and model research of movements of ground masses. In Proceedings of the European Congress on Ground Movement, The Hague, The Netherlands, 7–11 May 1948; University of Leeds: Leeds, UK, 1957; Volume 202.
27. Lu, J.; Yao, A.; Zheng, X. Study on the law and computational method of ground surface settlement induced by double-line tunnel excavation. *Chin. J. Rock Mech. Eng.* **2019**, *38* (Suppl. S2), 3735–3747.
28. Zienkiewicz, O.C.; Cheung, Y.K. *The Finite Element Method in Structural and Continuum Mechanics: Numerical Solution of Problems in Structural and Continuum Mechanics*; McGraw-Hill: New York, NY, USA, 1967.

29. Mase, L.Z.; Yundrismein, R.; Nursalam, M.A.; Putra, S.M.; Shelina, A.; Nugroho, S.H. A study of building performance inspection based on combination of site-specific response analysis and structural analysis (A case study of the Lighthouse View Tower in Bengkulu City, Indonesia). *Rud.-Geološko-Naft. Zb.* **2022**, *37*, 197–209. [[CrossRef](#)]
30. Hsiung, B.-C.B.; Likitlersuang, S.; Phan, K.H.; Pisitsopon, P. Impacts of the plane strain ratio on excavations in soft alluvium deposits. *Acta Geotech.* **2021**, *16*, 1923–1938. [[CrossRef](#)]
31. Shiri, Y.; Shiri, A. Discrete Fracture Network (DFN) Modelling of Fractured Reservoir Based on Geomechanical Restoration, a Case Study in the South of Iran. *Rud.-Geološko-Naft. Zb.* **2021**, *36*, 151–162. [[CrossRef](#)]
32. Vo-Minh, T.; Nguyen-Son, L. A stable node-based smoothed finite element method for stability analysis of two circular tunnels at different depths in cohesive-frictional soils. *Comput. Geotech.* **2021**, *129*, 103865. [[CrossRef](#)]
33. Liang, W.J.; Su, C.; Wangm, F.; Tang, X. Surrounding rock deformation analysis of underground caverns with multi-body finite element method. *Water Sci. Eng.* **2009**, *2*, 71–77.
34. Vazhbakht, B.; Zsaki, A.M. A finite element mesh optimization method incorporating geologic features for stress analysis of underground excavations. *Int. J. Rock Mech. Min. Sci.* **2013**, *59*, 111–119. [[CrossRef](#)]
35. Bao, X.; Wu, S.; Liu, Z.; Su, D.; Chen, X. Study on the nonlinear behavior of soil–pile interaction in liquefiable soil using 3D numerical method. *Ocean. Eng.* **2022**, *258*, 111807. [[CrossRef](#)]
36. Zhao, M.-H.; Liu, D.-P.; Zhang, L.; Jiang, C. 3D finite element analysis on pile-soil interaction of passive pile group. *J. Cent. South Univ. Technol.* **2008**, *15*, 75–80. [[CrossRef](#)]
37. Lade, P.V.; De Boer, R. The concept of effective stress for soil, concrete and rock. *Geotechnique* **1997**, *47*, 61–78. [[CrossRef](#)]
38. Sun, J. *Research and Application of Key Technology in Tunnel Structure Design*; People's Traffic Publisher: Beijing, China, 2017. (In Chinese)
39. *JTG D70-2004*; Chongqing Transportation Research and Design Institute. People's Republic of China Industry Standard JTG D70-2004: Code for Design of Highway Tunnels. People's Transportation Publishing House: Beijing, China, 2004. (In Chinese)
40. You, X.; Zhou, Q.; Xiao, Y.; Tong, L.; Yang, Q. Numerical Study on the Coupling Effect on a Retaining Structure of a Complex Deep Foundation Pit Group Excavation in a Soft-Soil Area. *Appl. Sci.* **2023**, *13*, 3263. [[CrossRef](#)]
41. Han, S.; Fan, C.; Zhou, A.; Ou, J. Simplified implementation of equivalent and ductile performance for steel-FRP composite bars reinforced seawater sea-sand concrete beams: Equal-stiffness design method. *Eng. Struct.* **2022**, *266*, 114590. [[CrossRef](#)]
42. Goldstein, R.V.; Dudchenko, A.V.; Kuznetsov, S.V. The modified Cam-Clay (MCC) model: Cyclic kinematic deviatoric loading. *Arch. Appl. Mech.* **2016**, *86*, 2021–2031. [[CrossRef](#)]
43. Li, B.; Wang, Z.Z. Numerical study on the response of ground movements to construction activities of a metro station using the pile-beam-arch method. *Tunn. Undergr. Space Technol.* **2019**, *88*, 209–220. [[CrossRef](#)]
44. Li, Z.; Lv, J.; Xie, X.; Fu, H.; Huang, J.; Li, Z. Mechanical characteristics of structures and ground deformation caused by shield tunneling under-passing highways in complex geological conditions based on the MJS method. *Appl. Sci.* **2021**, *11*, 9323. [[CrossRef](#)]

Disclaimer/Publisher's Note: The statements, opinions and data contained in all publications are solely those of the individual author(s) and contributor(s) and not of MDPI and/or the editor(s). MDPI and/or the editor(s) disclaim responsibility for any injury to people or property resulting from any ideas, methods, instructions or products referred to in the content.